

SinkSAM: A Monocular Depth-Guided SAM Framework for Automatic Sinkhole Segmentation

Osher Rafaeli[✉], Tal Svoray[✉] and Ariel Nahlieli[✉]

Abstract—Soil sinkholes significantly influence soil degradation, but their irregular shapes, along with interference from shadow and vegetation, make it challenging to accurately quantify their properties using remotely sensed data. We present a novel framework for sinkhole segmentation that combines traditional topographic computations of closed depressions with the newly developed prompt-based Segment Anything Model (SAM). Within this framework, termed SinkSAM, we highlight four key improvements: (1) The integration of topographic computations with SAM enables pixel-level refinement of sinkhole boundaries segmentation; (2) A coherent mathematical prompting strategy, based on closed depressions, addresses the limitations of purely learning-based models (CNNs) in detecting and segmenting undefined sinkhole features, while improving generalization to new, unseen regions; (3) Using Depth Anything V2 monocular depth for automatic prompts eliminates photogrammetric biases, enabling sinkhole mapping without the dependence on LiDAR data; and (4) An established sinkhole database facilitates fine-tuning of SAM, improving its zero-shot performance in sinkhole segmentation. These advancements allow the deployment of SinkSAM, in an unseen test area, in the highly variable semiarid region, achieving an intersection-over-union (IoU) of 40.27% and surpassing previous results. This paper also presents the first SAM implementation for sinkhole segmentation and demonstrates the robustness of SinkSAM in extracting sinkhole maps using a single RGB image.

Index Terms—Depth Anything V2, Sinkhole, YOLO, Drone, Segment Anything Model

I. INTRODUCTION

Piping erosion and soil sinkholes have a profound impact on landform evolution and soil degradation [1]. Many studies indicate that sinkholes can lead to irreversible damages to built areas, cause roads collapse, destroy farmlands, and induce dam piping [2]. Monitoring soil sinkholes occurrence, and characteristics, is crucial for studying dynamics of sinkhole-prone areas and mitigating sinkhole-related hazards.

Sinkholes manifest on the Earth’s surface as depressions, which can be observed either with the naked eye or through remote sensing (RS) platforms [3]. However, an automatic detection of soil sinkholes using RS imagery is still a challenging task that was tackled by several researchers so far [4]. The reasons for this research gap may be the fact that soil sinkholes are characterized by irregular shapes, suffer internal and external shadowing effect, can be masked by

vegetation and are usually spatially distributed over wide regions representing a typical imbalanced data problem [5].

To tackle these challenges, ancillary topographic information may be used to improve sinkholes segmentation in RS imagery. Data sources such as LiDAR (light detection and ranging), or photogrammetric Digital Elevation Models (DEMs) [6] were used for various topographic analyses. However, airborne LiDARs are rarely being used at high-resolution over wide regions, due to extremely high costs [7]. Photogrammetric DEMs can have low accuracy in representing terrain, as they often mistakenly capture vegetation or roof structures as part of the ground surface. They are also sensitive to lighting and shadows, with poor conditions potentially causing errors in elevation data. Compared with LiDAR-derived DEMs, photogrammetric models typically have limited vertical accuracy. Additionally, they struggle to capture steep terrain, as overlapping image pairs may not fully represent slope angles. Stereo matching issues can further result in gaps or distortions in the final DEM. [8].

As a substitute to these two topographic data sources, recently developed monocular depth estimation (MDE), using deep learning techniques, based on a single RGB image, became central in the field of computer vision [9]. MDE was proven useful in 3D reconstruction and target instance segmentation. However, in RS studies, MDE is still very rarely used [10], particularly geomorphological studies. This is unfortunate because MDE does not require multiple views as references, leading to improvements in both time and efficiency [11]. MDE was recently advanced with the Vision Transformer (ViT) based Depth anything V2 (DAV2) [12]. DAV2 outperformed similar Monocular Depth Estimation (MDE) foundation models, providing the most capable zero-shot MDE. DAV2 was benchmarked on the new diverse DA-2K dataset, which includes aerial photos and images with fine details, indicating its high potential for estimating terrain elevation from drones.

Automated sinkhole extraction using DEMs was applied based on topographic computations known as “fill sinks” algorithm [13]. Alternatively, authors applied machine learning techniques using geomorphometric variables, such as hillslope gradient and curvature, and topographic position [14], to detect areas prone to sinkholes [15].

The “fill sinks” method was successfully applied in various studies [6], [15], but the features extracted by this approach often suffer from overestimation and lack precision in delineating sinkhole boundaries. Consequently, depressions identified from topographic data frequently require refinement, usually through post-processing and visual inspection of RGB imagery

O. Rafaeli and A. Nahlieli are with the Department of Environmental, Geoinformatics and Urban Planning Sciences, Ben-Gurion University of the Negev, Israel (e-mail: osherr@post.bgu.ac.il; arielnah@post.bgu.ac.il).

T. Svoray is with the Department of Environmental, Geoinformatics and Urban Planning Sciences, and the Department of Psychology, Ben-Gurion University of the Negev, Israel (e-mail: tsvoray@bg.ac.il).

by humans [16].

Although may be inaccurate, advanced topographic information can enhance segmentation models, such as Convolutional Neural Networks (CNNs) [17]. CNNs typically capture semantic representations through stacked convolutions and pooling operations, followed by upsampling to restore image size [18]. Various encoder-decoder designs were applied to sinkhole segmentation [19], using DEMs and RGB images as inputs [20]. Performance of these models depends training datasets quality and the ability to generalize the models [21]. Due to the diverse appearance of sinkholes in S data, which hampers generalization, these models often struggle to be transferred effectively between different study areas [22].

Recently, foundational zero-shot models have become more commonly used in computer vision tasks [23], enhancing predictions by generalizing based on learning underlying data concepts and relationships, rather than being limited to detect set of classes from training data [24].

Meta FAIR (Fundamental AI Research) team gained progress with zero-shot prompt-based image segmentation during 2023-24, garnering considerable attention in RS fields [25]. ViT-based SAM may conduct image segmentation with minimal human intervention. SAM only requires a bounding box, or a clicked point, for a prompt [26]. Furthermore, when SAM is guided by models such as YOLO-generated box prompts [27], or is informed by other source to a region of interest, the entire segmentation pipeline can become end-to-end automatically [28]. These advancements in prompt-based classifiers and high-resolution depth estimation allow for the application of a new approach that leverages the close integration of "fill sinks" computations in image segmentation within an auto-prompt framework (Fig. 1).

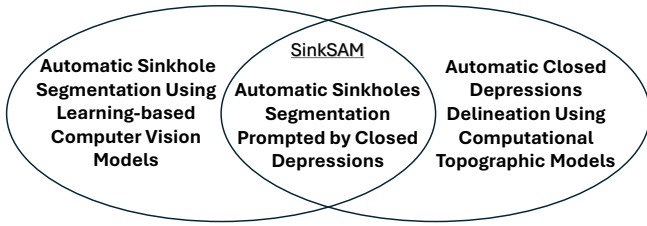


Fig. 1. Venn diagram illustrating the SinkSAM approach of merging Computational Topographic Models ("fill sinks") and purely learning-based computer vision models, using prompt technology.

Utilizing this synergy, we *aim* to improve sinkhole segmentation through a novel, fully-automatic framework named SinkSAM. Four operative objectives were set to achieve this aim: (1) automatically refining DEM-based computed closed depression boundaries with prompt-based segmentation of drone RGB imagery, thus addressing current requirements for visual inspection by human annotators; (2) overcoming generalization limitations of purely learning-based models by using a coherent mathematical prompting strategy through non-learnable closed depression computation; (3) comparing a photogrammetric DEM with deep learning-based DAV2 elevation estimation, to integrate the superior method into SinkSAM; and finally, (4) fine-tuning SAM using an estab-

lished sinkhole dataset to achieve high performance on an unseen study site, in a noisy semiarid environment.

II. RELATED WORK

A. Closed Depressions Computation for Sinkhole delineation

Topographic depressions, often known as closed depressions, can be extracted by subtracting elevation data of an original DEM from elevation data of a sink-free DEM [29]. The latter can be created using "fill sinks" algorithm as described by Planchon and Darboux in 2001 [30], Wang and Liu in 2006 [31], and by others [32]. In particular, the Planchon and Darboux algorithm was implemented in ArcGIS Pro as the "fill" tool.

"Fill sinks" was applied in many studies, for different real world conditions and sinkholes origins [6], [15], [33]. For example, it was applied to detect karst sinkholes in Kentucky using LiDAR DEMs with 1 m resolution, achieving a detection rate of 97% [34]. Others, utilized machine learning to improve detection accuracy of karst-origin sinkholes using high-resolution topographic information from LiDAR [14]. For example, logistic a regression model was applied to a dataset consisting morphometric characteristics derived from LiDAR-based topographic depressions, achieving an area under the curve (AUC) of 0.90 [35].

"Fill sinks" was also applied to small soil sinkholes induced by soil piping, in conjunction with derivatives of airborne LiDARs. Success rate was satisfactory on grasslands/pastures (76% for individual forms and 80% for piping systems). However, in areas with rough topography, it yielded lower identification rate for soil pipes (45% for individual forms and 50% for piping systems) [36].

To summarize, automatic sinkhole extraction methods from DEMs have two main limitations, both result in from the missing RGB information: (1) DEM-based methods tend to delineate non-sinkhole features that have a similar geometric representation in DEMs [15]; and (2) Sinkholes delineated from DEMs often have inaccurate boundaries [37], hampered by vegetation, mainly shrubs, within the sinkholes, consequently, DEMs often do not sufficiently represent the actual sinkhole structure [38]. To improve DEM-based methods, researchers often filter out such noisy features in post-processing with visual inspection of RGB imagery by human annotators [16].

B. Sinkhole Segmentation

Sinkhole segmentation was applied with CNN using RGB images [39]. In contrast with the topographic computations described in the previous section, which are physically-based, CNN-based segmentation, as a deep learning method, relies on training data quality and model generalization to similar tasks. Soil sinkhole segmentation is challenging compared with that of karst sinkholes, due to their amorphous shapes and the presence of objects in natural scenes that can be mistaken for sinkholes, such as shadows, vegetation, and other dark pixels [40]. Consequently, studies have reported only moderate accuracy for sinkhole detection, with Intersection over Union (IoU) values—as indicator of how well the model distinguishes

objects from background—ranging 20-60%, when evaluated on unseen areas, even for large sinkholes. [41], [42].

Most sinkhole segmentation studies have focused on model's architecture and input data used during training and testing. Input data included RGB images, DEMs and their derivatives, or combinations of the two sources [43]. For example, the implementation of a simple U-Net architecture has resulted in an IoU of 45.38% and Precision of 66.29% for karst sinkholes segmentation using LiDAR DEM and aerial imagery, with spatial resolution of 1.5 m [41]. It was also found that elevation gradient images as inputs, outperformed RGB imagery, because the latter provided weak cues for segmenting sinkholes. When applied to salt-induced, well-defined sinkholes, in drylands, an improved multi-class UNet using RGB-only aerial data proved promising, achieving IoU score of 97.08% (Drone) and F1 score of 91.23% (Satellite) [22]. However, for small soil sinkholes in semiarid regions, the Attention U-Net applied to RGB data, and elevation and its derivatives (e.g., hillshade, slope), from photogrammetric DEM, achieved optimal scores, with a relatively low IoU of 35.27% and a Precision of 53.98% [40].

C. Monocular Depth Estimation

Deep Learning-Based Monocular Depth Estimation (MDE) model allows to quantify depth from a single RGB image using training sets [9]. Most MDEs use an encoder-decoder architecture to minimize loss in training [44]. Depth estimation relies on cues such as: shading, occlusion, perspective, texture variations, and object scaling, to differentiate and understand the scene [45]. Monocular depth estimation was used for 3D reconstruction purposes, augmented reality, autonomous driving, and robotics [11].

Due to the limited payload capacity of most drones, they are typically outfitted with only a single camera. This prevents a widespread use of depth perception methods based on LiDAR or photogrammetric DEMs [46]. As an alternative, with the success of CNNs, MDEs have become increasingly reliable [47]. MDEs n attention in RS, while most studies were conducted in urban environments aimed at scene reconstruction with buildings [48], [49]. By contrast, MDEs are still rarely used [10], in studies of open environments and particularly of geomorphological processes in applications such as hillslope erosion processes, stream networks and sinkholes extractions.

Pre-trained Foundation Models have gained popularity in MDE tasks, being trained using large datasets and enabling zero-shot or fine tuning predictions [50]. In particular, DAV2 [12] introduces key advantages: (1) It overcomes limitations of image annotation by involving synthetic annotated data during training with fine detailed annotation; (2) It uses a teacher-student architecture to obtain a lightweight and accurate model. The model is trained on synthetic images. Then the teacher mode generates pseudo masks on unannotated real images. Finally, the smaller student model is trained on these pseudo-annotated images; (3) Its annotation pipeline incorporates AM for image sampling, utilizing a combination of real- and pseudo-labeled depth maps, from 62 million images [51].

DAV2 is benchmarked on standard datasets e.g., KITTI, Sintel, and more, outperforming previous Depth Anything version and the MiDas V3.1 from intel labs research [50]. A key highlight is DAV2's superior performance, when evaluated on the DA-2K dataset, which includes eight different image categories, 9% of which are aerial imagery and fine-detail images [12]. This indicates potential for terrain elevation estimation also from drone imagery. DAV2 was applied in a few studies of the open environment [52], for example, for agricultural canopy height measurements [53], providing a high performance solution, surpassing the current state-of-the-art.

D. Segment Anything Model

SAM is an encoder-decoder image segmentation model. SAM's encoder is a pre-trained Vision Transformer (ViT) with weights and biases trained by 1 Billion Mask (SA-1B) dataset [26]. Differently from traditional encoder-decoder models, SAM includes a prompt encoder [19] that is designed to use a human input of a point, or a bounding box, mapped as a vector embedding along with the image. SAM introduces three main advancements: (1) Promptable segmentation: SAM produces high-quality object masks from input prompts such as points or boxes; (2) It was trained on a dataset of 11 million images and 1.1 billion masks, created automatically by the model itself; (3) SAM exhibits strong zero-shot performance across a variety of segmentation tasks.

SAM was applied to image processing tasks, including medical image [54], shadow [55], and electron microscopy segmentation [56] crack segmentation [57] and road pit detection. In RS, SAM was also used for geological features analysis on planetary bodies [58], glacier segmentation [59], road mapping [60], building [61] and solar panels segmentation [62].

SAM models are trained and tested mostly by ground photographs and videos [63]. Due to unique properties of RS images, SAM still faces challenges when applied to RS in a zero-shot manner. When dealing with small objects, SAM may overestimate object size by including shadows in the segmented regions [64]. To achieve better performance on RS data, SAM needs to be fine-tuned to specific tasks. Fine-tuned variants of SAM perform better on aerial and satellite datasets compared with a non-fine-tuned SAM [65], [66].

Furthermore, when SAM is guided by computer vision prompts or other prompt generator [27], the entire process becomes automated. For example, YOLO [67], [68] and Grounding DINO [69] models were used to generate boxes to prompt SAM. Similarly, SAM may be informed by a non-learnable approach such as Topological Data Analysis (TDA) for optimized prompts with a reduced number of points to focus on regions of interest instead of applying a uniform grid across the entire cell in biological imaging [70].

III. MATERIALS AND METHODOLOGY

A. Study Area and Dataset

SinkSAM was applied to data from three agricultural catchments, in the northwestern Negev desert, east of the Mediterranean Sea coastline of Israel (Fig. 2). The climate is

semiarid with mean annual rainfall of 292 mm [71]. Soils are Late Pleistocene loess, with a sandy loam/silt loam texture [72]. Piping processes damaged many agricultural fields by induced sinkholes, resulting in a withdrawn of large areas from the cultivation cycle [73]. Sinkholes vary in their morphology, becoming irregular features with various dimensions (Fig 3). Some sinkhole's floors are covered by vegetation causing internal and external shadowing effects. The immediate surrounding of the sinkholes, being parts of agricultural fields, changes seasonally.

RGB data were collected by a drone in three sinkhole-prone subcatchments: Tel Gama (with $N=121$ soil sinkholes); Asaf ($N=226$); and Yaen ($N=216$). The drone survey was conducted using a DJI Phantom 4, equipped with Real-time Kinematic (RTK) technology, providing accurate images location and navigation data. The drone carried a 12 MP RGB camera and images were captured with 60% overlap from altitudes ranging 30-40 m to produce an orthomosaic and a DEM, using photogrammetry Agisoft Metashape with a pixel length of 0.025 m. Tel Gama and Asaf, containing approximately 350 sinkholes, were used as the training and validation sets, while Yaen, an unseen site, was reserved for testing. All ortomosaics were patchified to 512^2 px² patches (12^2 m²). Patches were overlaid by 50% (256 px stride) to ensure entire capture of sinkholes, at least in one patch.

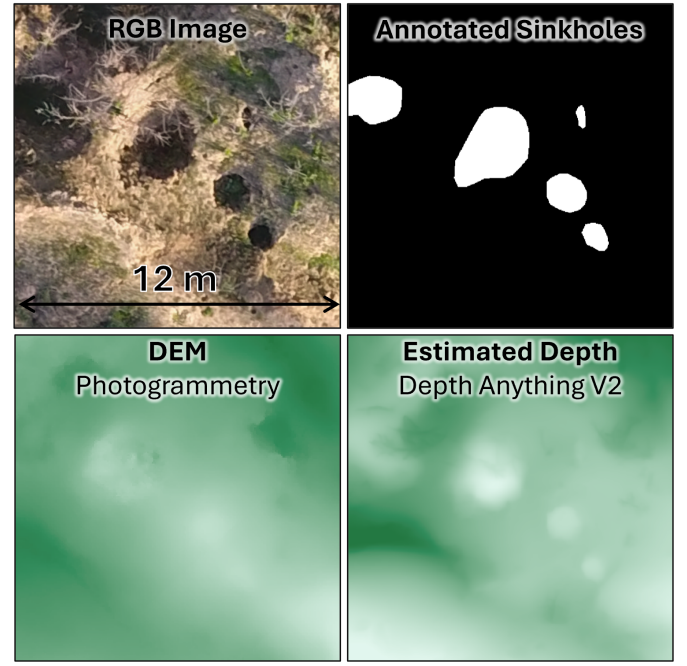


Fig. 3. Input data: Patches of RGB, ground truth annotated sinkholes, photogrammetric DEM and monocular depth estimated by DAV2. As can be seen in this patch, DAV2 correctly delineates sinkhole boundaries, while in photogrammetric DEMs, small sinkholes are neglected.

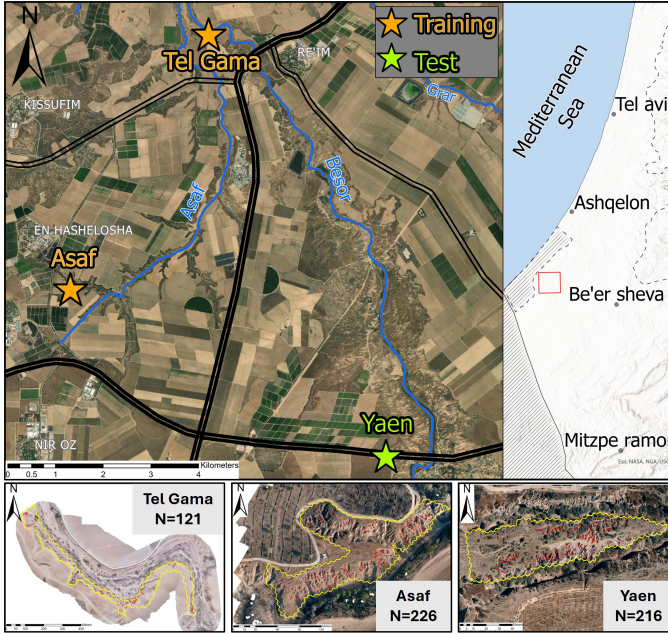


Fig. 2. The study area is located in the northwestern part of the Negev region, Israel. As shown below, the drone orthomosaic covers three sites prone to soil piping: Tel Gama and Asaf (Training), and Yaen (Test).

B. SinkSAM Framework Overview

The newly developed SinkSAM framework, for sinkhole detection and segmentation, is illustrated in Fig. 4. The framework consists four stages: *Stage 1*: depth estimation using DAV2 from a single RGB image; *Stage 2*: delineation of closed depressions. Done by: (1) "fill sinks" execution; and (2) the

subtraction of depth data of "as is" raster, from the "filled sinks" raster, using for both the depth data from stage 1; *Stage 3*: Prompts generation: a threshold is assigned to remove small sinks, and create bounding boxes from the depressions created in stage 2 for SAM usage in stage 4. Finally, *stage 4*: SAM utilizes an image encoder, and tuned mask decoder, for final segmentation of sinkholes.

Stage one - Monocular Depth Estimation: Orthomosaic patches were processed using pre-trained DAV2 model, based on a zero-shot model, with non-metric mode. Large Vision Transformer (ViT-L) encoder was used to achieve optimal accuracy in depth estimation. The patches preserved the same resolution, and geographic data, from the original RGB images, to ensure optimal alignment. We found, by simulations, that patch size of 512^2 px² is optimal for DAV2 estimation (Fig. 3).

Stage two - Closed Depressions Computation: The ArcGIS Pro "Fill" tool [74], was applied to fill all closed depressions of the DAV2 surface, up to their spill elevation (i.e. elevation at which water ideally flows out of the depression). This created a depression-less Depth map. The original DAV2 Depth data was then subtracted from the sinks-less raster to generate a difference raster representing depression location and depth.

Stage three - Prompts generation: The subtracted layer was filtered using two threshold values to erase small depressions. The threshold values were: depth < 2 (non-metric value) or area < 50 pixels. The subtracted rasters that were then unpatchified after filtering, reproduced a mosaic of closed depressions. Both raster layers, the RGB orthomosaic and the closed depression map, were then patchified again. Closed

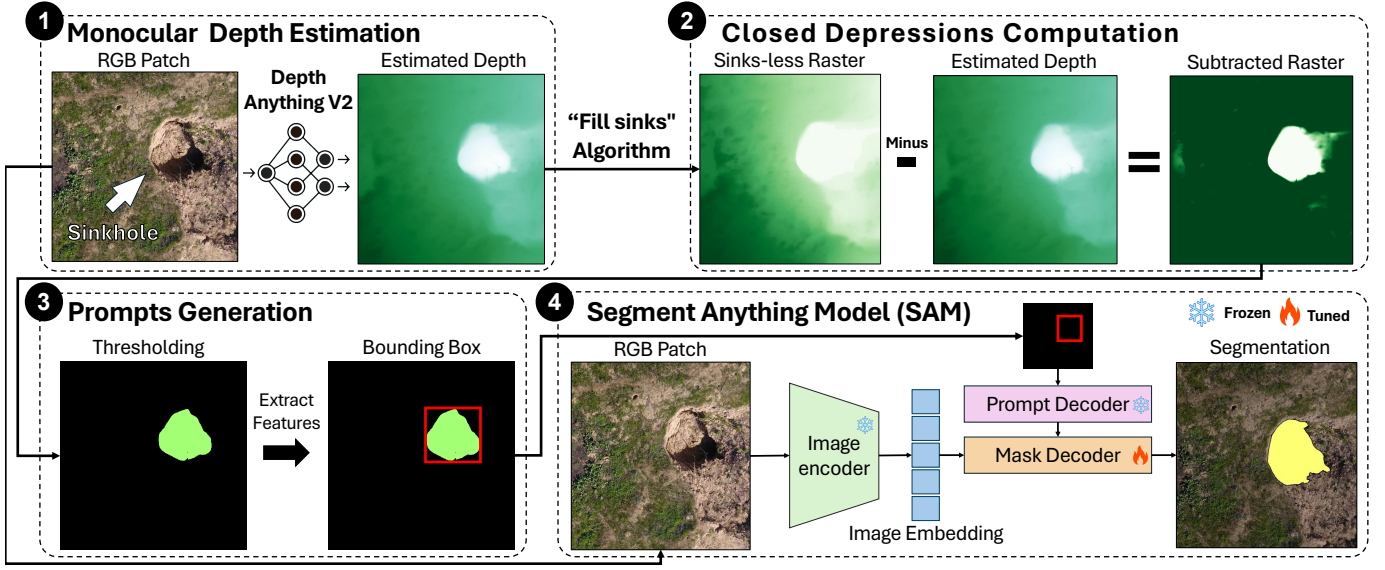


Fig. 4. SinkSAM framework: *Stage 1*: Depth estimation from an RGB image using DAV2. *Stage 2*: "Fill sinks" techniques and a subtraction of estimated depth from a sink-free raster resulting in delineation of closed depression. *Stage 3*: Prompts generation: a threshold value is used to remove small sinks and create bounding boxes for SAM. Finally, at *Stage 4*, the SAM tuned model utilizes an image encoder and mask decoder to create a final sinkholes map.

depressions in each patch were used to generate bounding boxes, in the next step to be used as SAM input along with corresponding RGB data.

Stage four - Segment Anything Model (SAM): RGB patches were processed by SAM, using the corresponding prompt box extracted from the depression layer (Stage 2). Masks were generated for each bounding box separately, and then all image predictions were combined. If more than one object appeared in a single image, predictions were combined by selecting pixels with highest foreground probability. The final evaluation has resulted in a referenced GIS layer of soil sinkholes.

IV. EXPERIMENTS

A. Experimental Setup

To evaluate SinkSAM's performance in sinkhole detection and segmentation, we compared it with other methods, on real world data, from an untested area. The experiment includes four comparisons that were specifically designed to test the performance of each of the four SinkSAM stages: (A) closed depressions, identified through the DEM-based closed depression method, and obtained at stage 2, before being used as prompts in SAM, are compared with sinkholes predicted by SAM, using these prompts. This comparison tests the entire SinkSAM framework against a DEM-based method; (B) prompt source: SAM prompted by closed depressions bounding boxes are compared with SAM prompted by YOLOv9 bounding boxes; (C) comparing DAV2 vs photogrammetric DEMs as elevation/depth input layers for the "fill sinks" algorithm, for testing their performance in sinkhole detection/segmentation accuracy; finally, (D) performance of SAM is compared with performance of tuned SinkSAM using bounding box prompts derived from DAV2 closed depressions.

B. Comparison between pairs

Comparison A - Computed Closed Depressions vs SAM:

This comparison was applied to validate the entire framework. It compares the depressions identified using the closed depression method by "fill sinks" with the final segmentation results from SAM. The aim is to determine whether image segmentation with SAM has added value within the integrated framework or the topographic computation is sufficient. Closed depressions, derived solely from depth data, were enclosed in bounding boxes and fed into SAM. This comparison allows to quantify SAM's role in refining the identified closed depressions.

Comparison B - Prompts Source: Two approaches for prompt generation were tested: (1) a learning-based model using NN; and (2) a non-learning, computation-based method, employing the "fill sinks" algorithm. For the learning-based approach, we used the widely-adopted YOLO end-to-end CNN for object detection [75]. The largest YOLOv9 model (YOLOv9e) was used to generate bounding boxes. YOLO was trained on data from Asaf and Tel Gama sites. These bounding boxes were used to prompt SAM, with a confidence threshold set at 0.2, which was found here optimal for this task.

Comparison C - Depth Data: To evaluate the first stage of SinkSAM, we compared DAV2 and a photogrammetric DEM as depth estimators. Both sources were tested for their accuracy in sinkholes segmentation based on computed depressions. Namely, we applied the "fill sinks" algorithm to extract closed depressions and assessed their quality in terms of sinkhole delineation. The extracted depressions were filtered by area and depth, removing features with area < 50 pixels. For depth, photogrammetric DEMs were thresholded at 2 cm, while for DAV2 we used a non-metric threshold of 2. This comparison did not involve variations in SAM configurations but we tested which depth source is more effective for bounding boxes usage by SAM.

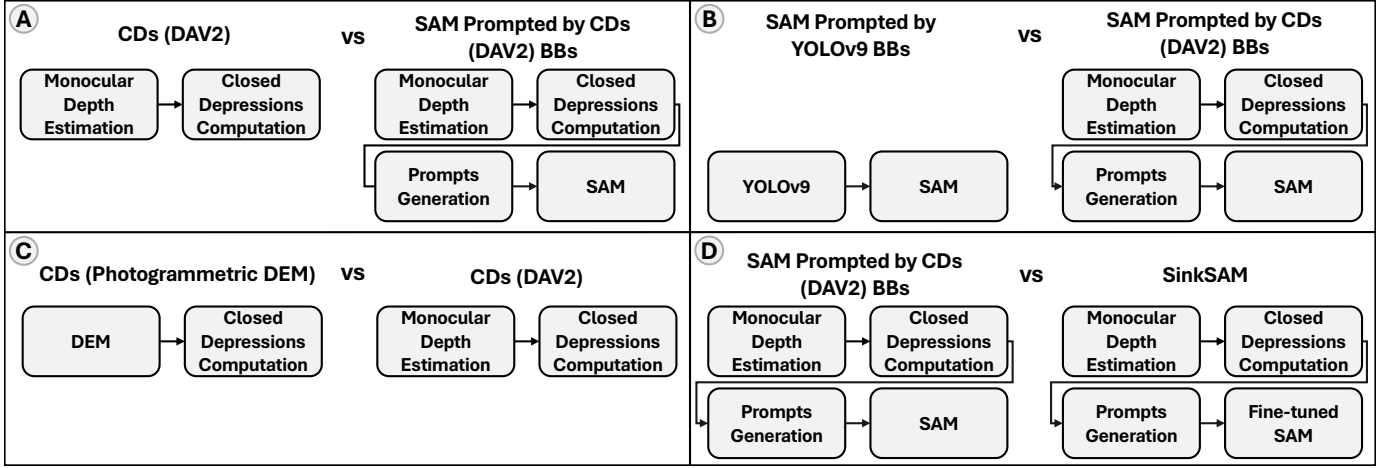


Fig. 5. Experimental setup: Each comparison was designed to test the performance of SinkSAM Framework: (A) closed depressions, identified through the Depth-based closed depression method vs sinkholes predicted by SAM, using these prompts. This comparison tests the entire SinkSAM framework against DEM-based method; (B) prompt source: SAM prompted by closed depressions bounding boxes vs SAM prompted by YOLOv9 bounding boxes; (C) comparing DAV2 vs photogrammetric DEMs as elevation/depth input layers for the “fill sinks” algorithm; finally, (D) performance of SAM is compared with performance of tuned SinkSAM using bounding box prompts derived from DAV2 closed depressions (CDs - Closed Depressions).

Comparison D - SAM Decoder: Zero-shot SAM and tuned SAM (SinkSAM) were executed, using bounding box prompts derived from DAV2 closed depressions. The goal was to quantify the impact of tuned SAM decoder, which was trained using our sinkhole inventory from the unseen Yaen site. The experimental setup allows for a comparison of each implementation configuration, with the better-performing components being integrated into the final SinkSAM framework (Fig. 5).

$$\begin{aligned}
 \text{Accuracy} &= \frac{TP + TN}{TP + FN + TN + FP} \\
 \text{Precision} &= \frac{TP}{TP + FP} \\
 \text{Recall} &= \frac{TP}{TP + FN} \\
 \text{F1 Score} &= 2 \times \frac{\text{Precision} \times \text{Recall}}{\text{Precision} + \text{Recall}} \\
 \text{IoU} &= \frac{|A \cap B|}{|A \cup B|}
 \end{aligned} \tag{2}$$

C. Implementation Details

Training Setting: SAM was fine-tuned using RGB images and annotated sinkholes, along with bounding boxes generated as masks to guide it during training. The model was fine-tuned using the large pretrained encoder (ViT-L). During the fine-tuning process, only parameters of SAM decoder were updated to adapt SAM to the sinkhole dataset. Freezing the encoder saves computational resources and allows larger batch size. In this fine-tuning process, we replicated the MedSAM project, which fine-tunes SAM on a dataset of medical images [76], and was inspired by the Encord AI teams [77].

Loss Function: A combination of the Binary Cross-Entropy Loss (L_{BCE}) and Dice Loss (L_{Dice}) was employed for training SAM mask decoder, as can be seen in Eq. 1:

$$L = L_{BCE} + L_{Dice} \tag{1}$$

Evaluation Metrics: To assess models performance, we employed the widely recognized evaluation metrics in Eq. 2:

where TP, TN, FP, and FN denote, respectively, the true positive, true negative, false positive, and false negative values, and A and B represent the predicted and ground truth segments, respectively. IoU denotes Intersection over Union.

The confusion matrix for object detection was used to evaluate a model’s performance by comparing predicted masks with ground truth masks, at different IoU thresholds. It quantifies detection rate at each IoU threshold. The confusion matrix categorizes the predictions into TP, FP, and FN based on the IoU threshold.

Technical details: We utilized high-performance computational resources to ensure efficient training and inference of segmentation models. Specifically, We employed the Ultralytics YOLOv8.2.71 framework [78] with PyTorch 2.3.1 for YOLO and SAM. For raster analysis, we used ArcPy site package that provides a useful and productive way to perform geographic data analysis [74]. All computations were executed using Python 3.9.15 with an NVIDIA RTX A4000 GPU. SAM and YOLOv9 were trained using the Adam optimizer, with a batch size of 4 images, for 25 epochs and 75 epochs, respectively, with learning rates of $1e-5$ and $2e-3$. The code for implementing SinkSAM is available on GitHub at the following link: <https://github.com/osherr1996/SinkSAM.git>.

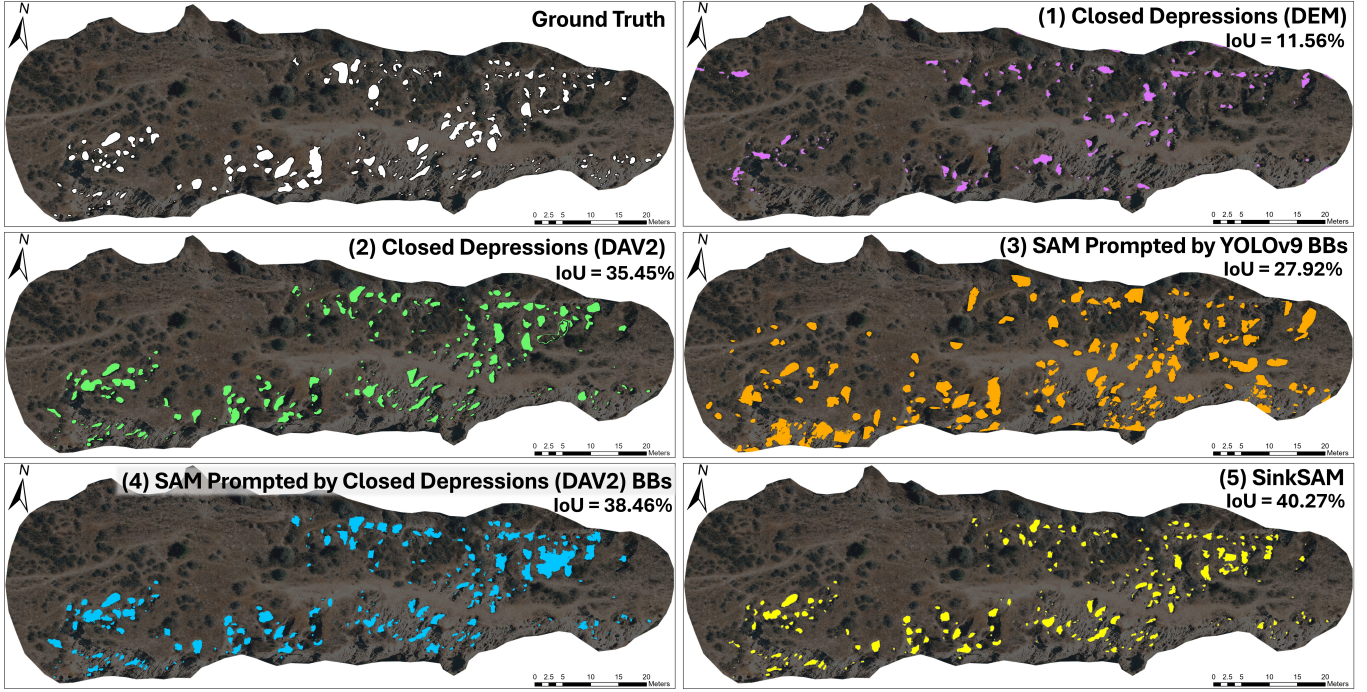


Fig. 6. Evaluated maps of sinkhole segmentation on the unseen Yaen site: It is visually evident that the photogrammetric closed depressions miss parts of the ground truth sinkholes, while DAV2 closed depressions delineate sinkholes more precisely. Regarding the segmentation models, SAM prompted by YOLO overestimates by segmenting parts of the background as sinkholes. Whereas, the SinkSAM map (with a tuned decoder) is the most similar to the ground truth map.

V. RESULTS

Model comparison results are illustrated using *five sinkhole maps* (Fig. 6) of the unseen Yaen site, which contains a total of 216 verified sinkholes. These include *two maps* of computed closed depressions generated using the “fill sinks” algorithm: Map 1 with a photogrammetric DEM as an input; and Map 2 with Depth Anything V2 (DAV2) as an input. The second batch consists of *three maps made by image segmentation*: Map 3 with SAM prompted by YOLOv9-generated boxes; Map 4 with SAM prompted by bounding boxes of closed depressions computed from DAV2 estimated depth; and Map 5 is SinkSAM with fine-tuned SAM prompted by bounding boxes of closed depressions computed from DAV2. The Results section highlights the key findings by presenting evaluation metrics from each pairwise comparison (Fig. 7).

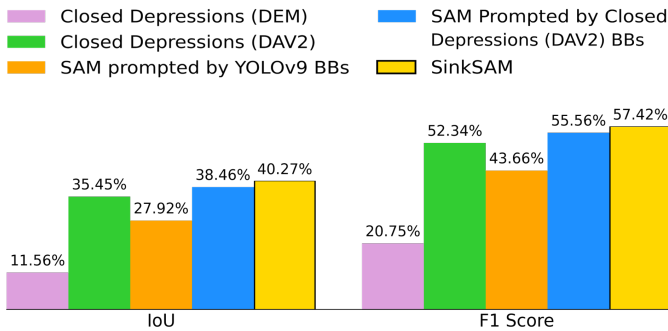


Fig. 7. Performance at different IoU thresholds: SinkSAM outperforms all models, while photogrammetric DEM achieves the lowest performance.

A. Closed Depressions by DAV2 using “fill sinks” vs Segmentation by SAM (Comparison A: Map 2 vs Map 4)

In this comparison, we assess the central concept of SinkSAM: the contribution of areas of interest, delineated by closed depressions derived from DAV2, using “fill sinks”, to SAM segmentation.

The results indicate that SAM indeed refines and improves segmentation in terms of pixel-level metrics, achieving an F1-Score of 55.56% compared with 52.34% for closed depressions, and an IoU of 38.46% compared with 35.45% for closed depressions. SAM reduces the increase rate of correctly segmented pixels, resulting in higher recall. Such improvement in matrices indicates that SAM prompted by these bounding boxes successfully refines the computed closed depressions process with the RGB sinkholes representation.

In terms of detection, SAM outperformed the “fill sinks” method, consistently achieving a higher true positive rate. The difference becomes more pronounced at higher IoU thresholds. For instance, at an IoU threshold of 30%, SAM correctly detected 112 sinkholes, while the “fill sinks” method identified only 92 out of the 216 actual sinkholes at the Yaen site, as shown in the confusion matrix. SAM’s ability to maintain a higher true positive rate at higher IoU thresholds further highlights its high performance.

A comparison of detection rates for the 216 sinkholes further highlights DAV2’s advantages. DAV2 allowed to successfully detect sinkholes, maintaining a high true positive (TP) rate across all IoU thresholds. In contrast, the use of photogrammetric DEM led to an underestimation of the sinkhole areas, resulting in a poor TP rate even at a low IoU

TABLE I
COMPARISON OF MODELS FOR SINKHOLE SEGMENTATION

Model\Method	Prompts Source	F1 (%)	IoU (%)	Pre. (%)	Rec. (%)	Acc. (%)
Closed Depressions Computation (DEM)	-	20.75%	11.56%	14.07%	39.47%	96.40%
Closed Depressions Computation (DAV2)	-	52.34%	35.45%	57.43%	48.08%	98.92%
SAM	YOLOv9 BB	43.66%	27.92%	33.54%	62.50%	95.02%
SAM	Closed Depressions (DAV2) BBs	55.56%	38.46%	52.91%	58.59%	98.55%
SinkSAM	Closed Depressions (DAV2) BBs	57.42%	40.27%	66.56%	50.49%	98.84%

threshold of 10% (138 true positives for DAV2 vs 38 for the DEM). At higher IoU thresholds, DAV2 continued to detect sinkholes, while the photogrammetric DEM’s detection rate dropped to zero at IoU thresholds $>40\%$ (see confusion matrix in Fig. 8).

B. Comparing Prompts: BBs from Closed Depressions (DAV2) vs BBs made by YOLOv9 (Comparison B: Map 3 vs Map 4)

This section presents an evaluation of SinkSAM’s prompt sources, comparing SAM prompted by DAV2-based closed depressions using the “fill sinks” method with SAM prompted by YOLOv9. Specifically, we analyze the performance of these two prompt types in detecting and segmenting sinkhole boundaries using SAM.

The results demonstrate that bounding boxes from DAV2 closed depressions provide more reliable prompts for SAM. For pixel-level segmentation, SAM prompted by closed depression bounding boxes achieved an F1-Score of 55.56%, compared with 43.66% for SAM prompted by YOLOv9, and an IoU of 38.46%, compared to 27.92% for YOLOv9-prompted SAM. YOLOv9 tended to overestimate sinkhole detection, causing SAM to segment more background, which resulted in false positive boxes being fed into SAM and leading to inaccurate object segmentation, as reflected in its low precision of 33.54%.

At lower IoU thresholds, SAM prompted by closed depression bounding boxes significantly outperformed SAM prompted by YOLOv9. For example, at a 20% IoU threshold, YOLOv9 incorrectly detected 106 sinkholes, while SAM with closed depression prompts misidentified only 89. Using same threshold, YOLOv9 missed 124 sinkholes, compared with 90 missed by SAM with closed depression prompts, and 78 missed by SinkSAM (see Fig. 8). Although YOLOv9-detected sinkholes showed a smaller drop in true positive rates at higher IoU thresholds, it still had a high number of undetected sinkholes, with 146 false positives at a 50% IoU threshold. Additionally, YOLOv9 falsely detected a large number of non-sinkholes as sinkholes.

C. Photogrammetric DEM vs DAV2 (Comparison C: Map 1 vs Map 2)

DAV2 significantly outperformed the photogrammetric DEM as an input data to delineate close depressions using “fill sinks” algorithm. The photogrammetric DEM was observed as too smooth with lower differences, between grid-cell values in the immediate vicinity of the depressions, than DAV2. Depressions delineated by DAV2 achieved an F1-Score of 52.34%,

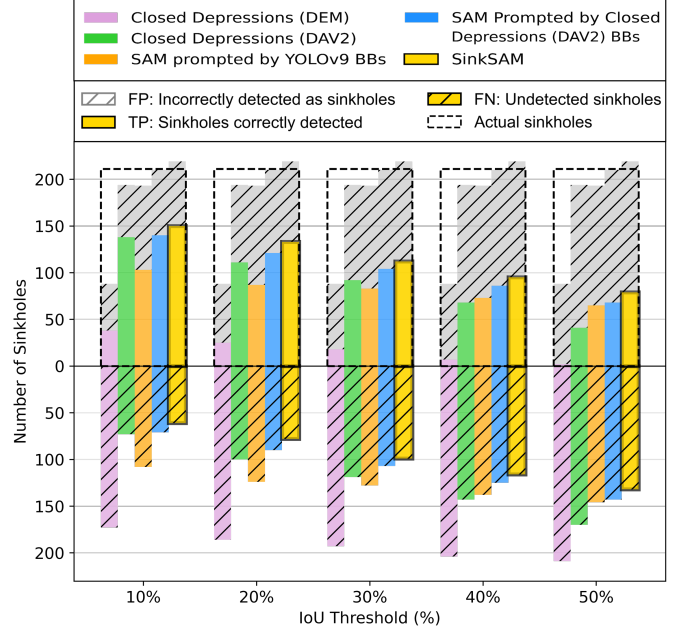


Fig. 8. Performance of sinkhole detection models: A bar plot of the confusion matrix illustrates the performance of various models over IoU thresholds in an unseen test area. The tested area, known as the Yaen site, contains 216 ground truth sinkholes. SinkSAM outperforms all other models, while the closed depression computation using photogrammetric DEM achieved the lowest performance.

while those based on the photogrammetric DEM achieved only 20.75%. DAV2 enabled the detection of small depressions, which were clearly overlooked by the photogrammetric DEM, as can be observed in the maps (see Fig. 6). DAV2 provided also a more precise delineation of the sinkhole boundaries. These differences led to improved segmentation performance when using DAV2 as input, achieving an IoU of 35.35%, compared to the photogrammetric DEM’s significantly lower IoU of just 11.56%.

D. SAM vs Fine-tuned SAM (SinkSAM) (Comparison D: Map 4 vs Map 5)

The final version of SinkSAM, which includes a fine-tuned SAM decoder, prompted by closed depression bounding boxes derived from DAV2, was assessed here. Fine-tuning the decoder parameters of the zero-shot SAM for the sinkhole detection task led to enhanced performance in both the segmentation and detection of sinkholes.

SinkSAM outperformed in segmentation accuracy, achieving an F1-Score of 57.42%, while the zero-shot SAM achieved

55.56%. SinkSAM also reached an IoU of 40.27%, compared with 38.46% for the un-tuned SAM. High false positive rate led to a significant difference in precision, with SinkSAM achieving 66.56%, while SAM only achieved 52.91% (Table I).

In terms of sinkhole detection, SinkSAM outperformed SAM by maintaining fewer false positives and false negatives across all IoU thresholds, as demonstrated in the confusion matrix (Fig. 8). For instance, at an IoU threshold of 30%, SinkSAM correctly detected 112 sinkholes, compared to SAM's 104 out of 216. At a 50% threshold, SinkSAM accurately identified 79 sinkholes, while SAM detected only 68. This experiment highlights that SinkSAM surpassed all other versions evaluated in the current study in both segmentation and detection.

VI. DISCUSSION

The series of experiments conducted in this study showcases the key features of SinkSAM: (1) an automatic refinement of closed depressions via pixel-level RGB image segmentation; (2) prompting by closed depressions using digital elevation data; (3) an integration of monocular depth in sinkhole segmentation; and (4) fine-tuning of SAM using a high-resolution and well-established sinkhole database. These findings underscore SinkSAM's potential to address the limitations of previous sinkhole segmentation methods.

A. Refinement of Closed Depressions by RGB data

The DEM-based sinkhole delineation method, "fill sinks," became widely utilized in topographic analysis and geomorphometric applications. Its integration into ArcGIS Pro GIS software made it accessible to a broad range of researchers, engineers, and soil conservationists for various purposes [6], [15], [79]. As was discussed in the *Related Work* section, this usage of DEM-based sinkhole delineation methods, without the support of RGB data, introduces two challenges: (1) false detection of non-sinkhole features [15]; and (2) inaccurate segmentation of sinkhole boundaries [38].

Consistent with previous achievements, our results demonstrate that closed depressions delineated using "fill sinks" tend to under- or over-estimate the sinkhole boundaries. This leads to larger or smaller sinkhole area coverage than actual, resulting in many incorrectly segmented pixels. On the other hand, the integration of SinkSAM with automatic prompting, using computed closed depressions from 3D data as bounding boxes, allowed for pixel-level segmentation. This approach enhanced sinkhole detection and delineation compared to traditional DEM-based methods (see Fig. 9). That is because SinkSAM facilitates an automatic refinement of sinkhole boundaries, using an RGB true representation. An attempt to achieve that level of precision of SinkSAM, was previously accomplished only through manual inspection of RGB imagery by human annotators [80]. This was done post-processing, after the stage of topographic computations had ended [37].

By applying SAM, sinkhole segmentation was improved, with an increased IoU (from 35.45% for the "fill sinks" algorithm to 38.46% for SAM and 40.27% for SinkSAM).

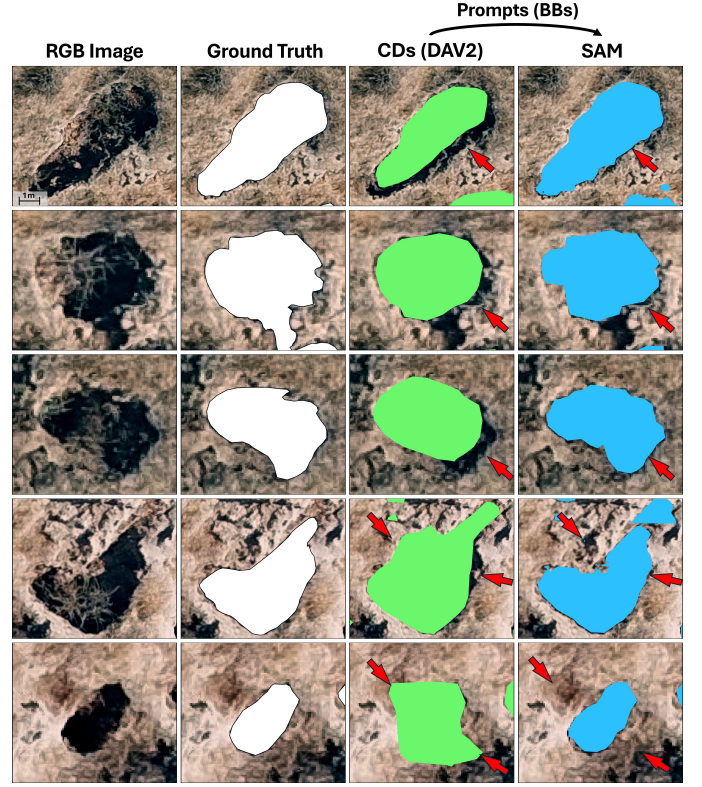


Fig. 9. SAM prompted by closed depressions: SAM improved sinkhole segmentation, although closed depressions (DAV2) tend to either overestimate or underestimate sinkhole areas, leading to inaccurate bounding boxes. SAM (zero-shot), especially when prompted with smaller boxes, effectively refines the output, providing more accurate delineation of actual sinkholes (CDs - closed Depressions).

This improvement is evident both when using large bounding boxes, that include both sinkholes and background, or smaller ones that partially capture sinkholes (Fig. 9). Nonetheless, when SinkSAM was prompted by non-sinkhole features, the machine did not always filter out false positives. Instead, it often refined them by assigning low confidence. Yet, when non-sinkhole black pixels that resemble sinkholes were involved, this led to erroneous object segmentation. Future work should focus on improving prompt generation from depth information filtered based on shape and area to differentiate true sinkholes [81], and more integrated advanced approaches with information on slope, curvature, and other indices to improve precision [14], [35].

B. Closed Depressions Prompting

Incorporating "fill sinks" computation with automatic prompting addresses the shortcomings of fixed learning models in identifying undefined sinkhole features and transferring knowledge to new areas (see Fig. 11). The performance of learnable segmentation models, such as CNNs, in handling similar tasks after training is influenced by two key factors: the model's ability to recognize relevant patterns and the diversity and representativeness of training data [82]. Sinkholes often present a challenge in both aspects, because many studies rely on unseen, natural data, leading to moderate accuracy, with

IoU values ranging 20%-60%, even for large sinkholes [42]. Particularly, sinkholes segmentation performance declined in a highly variable semiarid region with small and undefined soil piping sinkhole. As reported in these regions, an improved multi channel U-Net achieved an optimal IoU of 35.27% [40]. See reports in previous studies on relatively low sinkhole segmentation performance in the *Related Work* section.

Soil piping sinkholes exhibit significant morphological variation [83], leading to differing visual appearances (see Fig. 10). This often causes CNN-based models to misidentify shadows and shrubs as sinkholes, leading to errors and difficulties in generalizing to new, unseen data [84]. This issue was also confirmed by us, where YOLO frequently overestimated sinkholes due to the presence of dark pixels from other objects, resulting in false positives (see Table I).

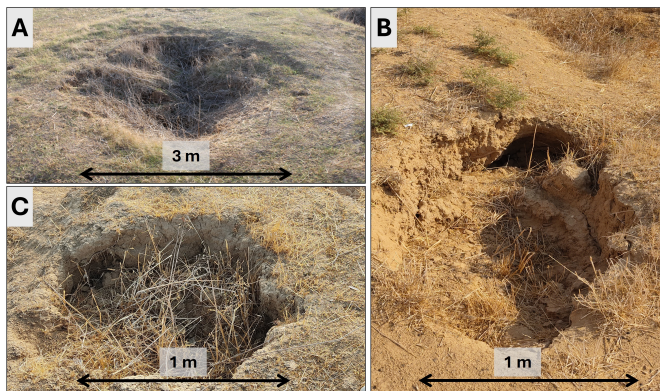


Fig. 10. Ground level sinkholes images from study area: Sinkholes can vary in their morphology, resulting in irregular features with different dimensions. Additionally, the base of a sinkhole's appearance varies: some sinkhole are deep, resulting in a dark, shadowy appearance (b), while others are filled with collapsed soil, creating a bright appearance at the bottom (a). Moreover, some sinkholes contain vegetation inside them (c).

To address this bias, we adopted a non-learnable prompting approach that has the potential to generalize more effectively to new tasks. A similar method was successfully applied in the biological imaging field, where function values were used to identify local image extreme. These peaks marked the locations of cells, serving as prompts for SAM [70]. It was emphasized that computation-based automatic prompting is less likely to produce inconsistent or unstable decisions compared with fixed learning methods.

SinkSAM integrates the non-learnable "fill sinks" algorithm with RGB segmentation to accurately extract sinkhole masks. This non-learnable prompting strategy overcomes the wide variation in sinkhole appearances and the lack of robustness in CNN models when transferring to new areas, achieving significantly higher IoU (38.46% for zero-shot SAM prompted by closed depression bounding boxes compared to 27.92% for SAM prompted by YOLO bounding boxes).

C. Monocular Depth Estimation

Depth information can be an essential data source for accurate sinkhole segmentation and detection. Yet, high-resolution DEMs are not always readily available [7]. LiDAR, while providing high-resolution and accurate elevation data, is rarely

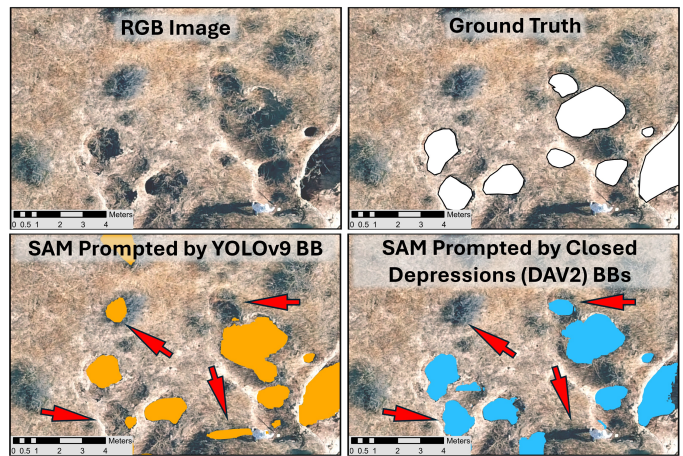


Fig. 11. Closed depressions prompting: YOLO overestimates by incorrectly detecting non-sinkhole dark pixels (such as shadows and shrubs) as sinkholes. In contrast, closed depressions calculated from DAV2 provide more reliable prompts to SAM.

used at the local scale due to its high cost. Conversely, as was shown in the *Related Work* section, low resolution LiDARs are not usable for sinkhole segmentation. For instance, a 1 m airborne LiDAR DEM was found inadequate for detecting small soil piping-related sinkholes [36]. Photogrammetric DEMs are more accessible, but they often suffer inaccuracies and misalignment with orthomosaics, which can lead to an underrepresentation of sinkholes, making them less reliable for segmentation or even creating accurate topographic models [8].

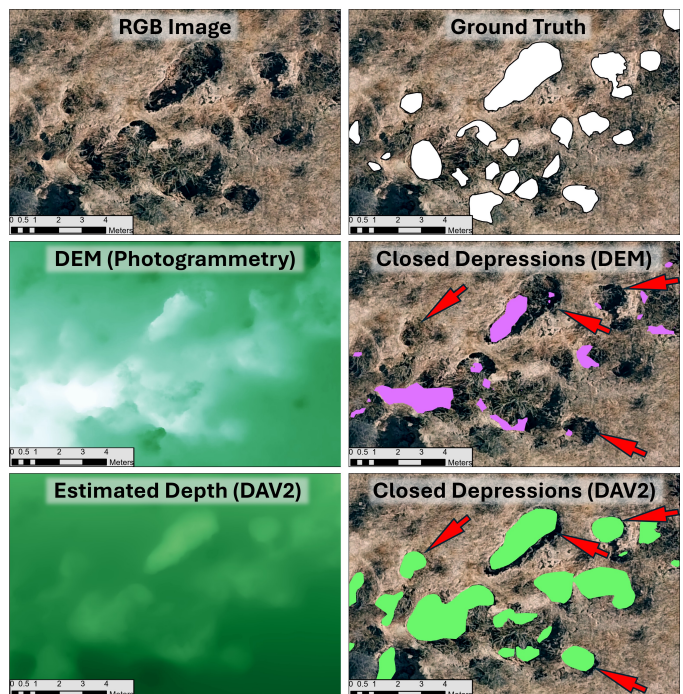


Fig. 12. Photogrammetric DEM vs DAV2: Sinkholes delineation from evaluated maps, compared to the ground truth sinkhole masks, DAV2 closed depressions delineate the boundaries more precisely and "fill" the entire area of the sinkholes, while DEM closed depressions only "fill" parts of the sinkholes and do not fill small sinkholes at all.

Similar to previous observations, we addressed inaccuracies in sinkhole detection encountered with photogrammetric DEMs. To improve upon this, we used MDE (Monocular Depth Estimation) foundation models, which have gained traction in depth estimation tasks by enabling zero-shot or fine-tuning predictions [50]. Notably, the state-of-the-art DAV2 model has delivered impressive results across multiple datasets, including aerial imagery, outperforming equivalent foundation models [12]. Since its introduction, DAV2 was applied in agricultural canopy height measurements [53], offering a highly efficient and high-performing solution that surpasses current methods with superior or comparable accuracy.

Our findings demonstrate that DAV2, even in its zero-shot configuration, excels in depth estimation using a single RGB drone image as an input. DAV2 allowed to detect fine sinkholes missed by photogrammetric DEMs, as is evident in the elevation profiles (Fig. 13). DAV2 also provided more precise delineation of sinkhole boundaries (Fig. 12). DAV2's depth maps are aligned geometrically with an RGB image, eliminating small offsets typically found in photogrammetric DEMs and ultimately generating more accurate prompts for SAM.

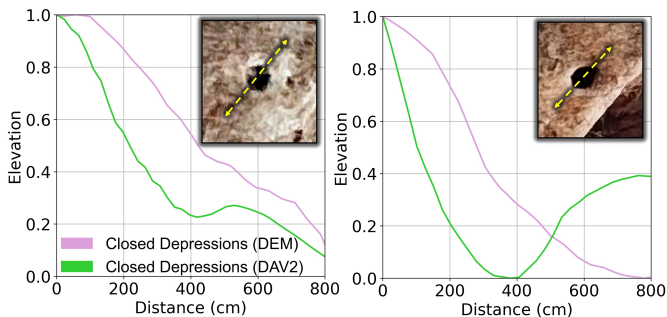


Fig. 13. Monocular depth estimation: Elevation profile plots on small sinkholes. Note that DAV2 captures small sinkholes that the photogrammetric DEM fails to detect causing under estimation of sinkholes.

The current paper marks the first application of DAV2, on drone imagery, for detecting geomorphic features of interest. Specifically, it is the first time a raster-based algorithm has been applied to monocular depth estimation for geomorphic feature extraction, a process that traditionally done using LiDAR or photogrammetric DEMs [29]. DAV2 can be further fine-tuned on drone imagery for even more accurate sinkhole depth estimation and can also be switched to metric mode, enabling it to extract both the geometric dimensions and boundaries of sinkholes.

D. Fine-tuned SAM

A large sinkhole database, which includes 350 mapped sinkholes, was captured using high-resolution RGB drone imagery, by human annotators. This data enabled efficient fine-tuning of SAM, significantly improving its performance in sinkhole segmentation. As was shown in our experimental results, SinkSAM reduced the number of misclassified background pixels compared with the zero-shot SAM, (Fig. 14).

Zero-shot SAM was applied in RS studies with promising results [25]. For instance, it was used to segment glaciers and geological features in a zero-shot setting [58], [59]. However, Zero-shot SAM is prone to over-segmentation, especially when object boundaries are amorphous and therefore unclear [85]. This is a methodological challenge because many objects on the Earth surface are amorphous and hard to segment from RS data. Consequently, fine-tuning is often necessary for segmentation tasks in this domain. Studies have already showed that fine-tuning improves segmentation accuracy by SAM for roads and buildings in RS imagery [25], [60].

In line with these findings on different objects, SAM's performance in sinkhole segmentation here is reasonable in zero-shot mode, but, it tended to segment parts of the background, such as shadows and shrubs, leading to a higher false positive rate, especially when object boundaries were fuzzy. By fine-tuning the decoder on the sinkhole dataset, we observed improvements similar to those seen with medical imagery datasets [76]. Further improvements in SinkSAM are possible with fine-tuning on a larger sinkhole database, which would help generalize its application to a wider variety of sinkholes from different origins.

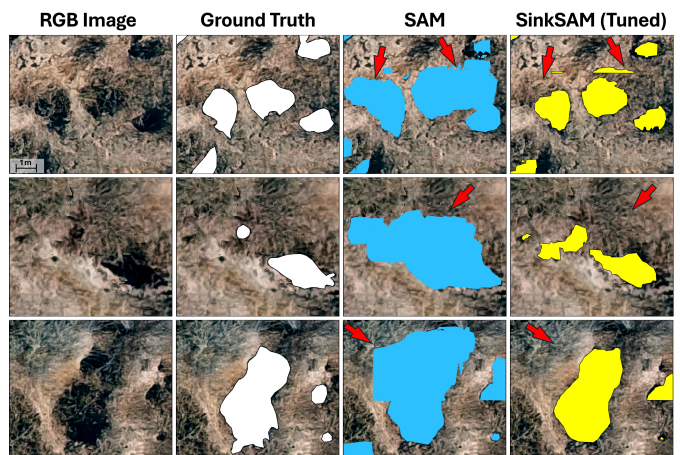


Fig. 14. SAM vs Fine-tuned SAM: Fine-tuned SAM significantly improved segmentation performance. Zero-shot SAM tends to segment non-sinkholes, especially when prompted with large bounding boxes that capture non-sinkhole objects in the background or sinkholes boundaries is not well defined. This bias results in lower precision compared to the fine-tuned model.

VII. CONCLUSION

This paper formulates a novel automatic SAM framework, called SinkSAM, for segmenting soil sinkholes from a single RGB image. It integrates "fill sinks" computation with prompt-based SAM segmentation, effectively handling environments obscured by vegetation cover and shade.

A series of four experiments established clearly the higher performance of SinkSAM compared with previous methods: (1) SinkSAM yielded pixel-level refinement of traditional DEM-based closed depression computation by adding RGB data; (2) Integrating "fill sinks" output data to automatic prompting allowed to overcome limitations of CNN-based learnable sinkhole detection (e.g., YOLO) and enhanced sinkhole segmentation by identifying undefined sinkhole features

and model transfer successfully to unseen sites; (3) The use of automatic prompts based on monocular depth, with a single RGB image only, allowed to overcome photogrammetric DEM biases and made sinkhole mapping feasible without using expensive LiDAR data. DAV2 demonstrated its strength as an AI-based substitute for 3D data input for "fill sinks", providing useful SAM prompts; and (4) The established sinkhole database allows fine-tuning of SAM, improving its segmentation performance.

These results position SinkSAM as a generalized, and an accessible, framework for sinkhole segmentation. SinkSAM framework may be applied for agricultural land management, geological research, hazard mapping and risk assessment, and early warning systems. It can also be improved in three key areas: (1) improving prompt generation from depth information by employing more advanced computational methods, or topographic indices, combined with classifiers, to reduce over-estimation and generate more reliable prompts for SinkSAM; (2) implementing SinkSAM with LiDAR data to compare model performance with DAV2 usage; and (3) fine-tuning SinkSAM on a larger sinkhole database to generalize its application to a variety of sinkholes from different origins.

ACKNOWLEDGMENT

We thank the Ministry of Agriculture Chief Scientist, grant number 16-17-0005, 2022, and the Negev Scholarship by the Kreitman School of Ben-Gurion University of the Negev that support Osher Rafaeli's PhD studies.

REFERENCES

- [1] J. De Waele, F. Gutiérrez, M. Parise, and L. Plan, "Geomorphology and natural hazards in karst areas: A review," *Geomorphology*, vol. 134, no. 1, pp. 1–8, 2011. *Geomorphology and Natural Hazards in Karst Areas*.
- [2] T. Waltham, F. Bell, and M. Culshaw, "Sinkholes and subsidence: Karst and cavernous rocks in engineering and construction," *Springer-Praxis*, 01 2005.
- [3] F. Gutiérrez, J. P. Galve, P. Lucha, C. Castañeda, J. Bonachea, and J. Guerrero, "Integrating geomorphological mapping, trenching, insar and gpr for the identification and characterization of sinkholes: A review and application in the mantled evaporite karst of the ebro valley (ne spain)," *Geomorphology*, vol. 134, no. 1-2, pp. 144–156, 2011.
- [4] F. Gutierrez, A. H. Cooper, and K. S. Johnson, "Identification, prediction, and mitigation of sinkhole hazards in evaporite karst areas," *Environmental Geology*, vol. 53, pp. 1007–1022, 2008.
- [5] A. Bernatek-Jakiel and J. Poesen, "Subsurface erosion by soil piping: significance and research needs," *Earth-Science Reviews*, vol. 185, pp. 1107–1128, 2018.
- [6] E. Pardo-Igúzquiza and P. Dowd, "The mapping of closed depressions and its contribution to the geodiversity inventory," *International Journal of Geoheritage and Parks*, vol. 9, no. 4, pp. 480–495, 2021.
- [7] S. Hummel, A. Hudak, E. Uebler, M. Falkowski, and K. Megown, "A comparison of accuracy and cost of lidar versus stand exam data for landscape management on the malheur national forest," *Journal of forestry*, vol. 109, no. 5, pp. 267–273, 2011.
- [8] M. Uysal, A. Toprak, and N. Polat, "Dem generation with uav photogrammetry and accuracy analysis in sahitlek hill," *Measurement*, vol. 73, pp. 539–543, 2015.
- [9] C. Zhao, Q. Sun, C. Zhang, Y. Tang, and F. Qian, "Monocular depth estimation based on deep learning: An overview," *Science China Technological Sciences*, vol. 63, no. 9, pp. 1612–1627, 2020.
- [10] V.-C. Miclea and S. Nedeveschi, "Dynamic semantically guided monocular depth estimation for uav environment perception," *IEEE Transactions on Geoscience and Remote Sensing*, vol. 62, pp. 1–11, 2024.
- [11] Y. Ming, X. Meng, C. Fan, and H. Yu, "Deep learning for monocular depth estimation: A review," *Neurocomputing*, vol. 438, pp. 14–33, 2021.
- [12] L. Yang, B. Kang, Z. Huang, Z. Zhao, X. Xu, J. Feng, and H. Zhao, "Depth anything v2," 2024.
- [13] A. Sharma and K. Tiwari, "Sink removal from digital elevation model—a necessary evil for hydrological analysis," *Current science*, vol. 117, pp. 1512–1515, 11 2019.
- [14] J. Zhu, A. M. Nolte, N. Jacobs, and M. Ye, "Using machine learning to identify karst sinkholes from lidar-derived topographic depressions in the bluegrass region of kentucky," *Journal of Hydrology*, vol. 588, p. 125049, 2020.
- [15] J. Hofierka, M. Galloway, P. Bandura, and J. Šašák, "Identification of karst sinkholes in a forested karst landscape using airborne laser scanning data and water flow analysis," *Geomorphology*, vol. 308, pp. 265–277, 2018.
- [16] C. Ferreira, Y. Hussain, R. Uagoda, T. Silva, and R. Cicerelli, "Uav-based doline mapping in brazilian karst: A cave heritage protection reconnaissance," *Open Geosciences*, 10 2023.
- [17] Q. Yuan, H. Shen, T. Li, Z. Li, S. Li, Y. Jiang, H. Xu, T. Weiwei, Q. Yang, J. Wang, J. Gao, and L. Zhang, "Deep learning in environmental remote sensing: Achievements and challenges," *Remote Sensing of Environment*, vol. 241, p. 111716, 05 2020.
- [18] O. Ronneberger, P. Fischer, and T. Brox, "U-net: Convolutional networks for biomedical image segmentation," *CoRR*, vol. abs/1505.04597, 2015.
- [19] X. X. Zhu, D. Tuia, L. Mou, G.-S. Xia, L. Zhang, F. Xu, and F. Fraundorfer, "Deep learning in remote sensing: A comprehensive review and list of resources," *IEEE Geoscience and Remote Sensing Magazine*, vol. 5, no. 4, pp. 8–36, 2017.
- [20] N. V. Hoai, N. M. Dung, and S. Ro, "Sinkhole detection by deep learning and data association," in *2019 Eleventh International Conference on Ubiquitous and Future Networks (ICUFN)*, pp. 211–213, 2019.
- [21] P. Sharma, Y. P. S. Berwal, and W. Ghai, "Performance analysis of deep learning cnn models for disease detection in plants using image segmentation," *Information Processing in Agriculture*, vol. 7, no. 4, pp. 566–574, 2020.
- [22] O. Alrabayah, D. Caus, R. A. Watson, H. Z. Schulten, T. Weigel, L. Rüpke, and D. Al-Halbouni, "Deep-learning-based automatic sinkhole recognition: Application to the eastern dead sea," *Remote Sensing*, vol. 16, no. 13, p. 2264, 2024.
- [23] T. Lüddecke and A. Ecker, "Image segmentation using text and image prompts," in *Proceedings of the IEEE/CVF Conference on Computer Vision and Pattern Recognition (CVPR)*, pp. 7086–7096, June 2022.
- [24] S. Liu, Z. Zeng, T. Ren, F. Li, H. Zhang, J. Yang, Q. Jiang, C. Li, J. Yang, H. Su, J. Zhu, and L. Zhang, "Grounding dino: Marrying dino with grounded pre-training for open-set object detection," 2024.
- [25] L. P. Osco, Q. Wu, E. L. de Lemos, W. N. Gonçalves, A. P. M. Ramos, J. Li, and J. M. Junior, "The segment anything model (sam) for remote sensing applications: From zero to one shot," 2023.
- [26] A. Kirillov, E. Mintun, N. Ravi, H. Mao, C. Rolland, L. Gustafson, T. Xiao, S. Whitehead, A. C. Berg, W.-Y. Lo, P. Dollár, and R. Girshick, "Segment anything," 2023.
- [27] J. Redmon, S. Divvala, R. Girshick, and A. Farhadi, "You only look once: Unified, real-time object detection," in *2016 IEEE Conference on Computer Vision and Pattern Recognition (CVPR)*, pp. 779–788, 2016.
- [28] Y. Zhu, Q. Yang, and L. Xu, "Active learning enabled low-cost cell image segmentation using bounding box annotation," 2024.
- [29] V. Zumpano, L. Pisano, and M. Parise, "An integrated framework to identify and analyze karst sinkholes," *Geomorphology*, vol. 332, pp. 213–225, 2019.
- [30] O. Planchon and F. Darboux, "A fast, simple and versatile algorithm to fill the depressions of digital elevation models," *CATENA*, vol. 46, no. 2, pp. 159–176, 2002.
- [31] L. Wang and H. Liu, "An efficient method for identifying and filling surface depressions in digital elevation models for hydrologic analysis and modelling," *International Journal of Geographical Information Science*, vol. 20, no. 2, pp. 193–213, 2006.
- [32] L. Yong-He, Z. Wan-Chang, and X. Jing-Wen, "Another fast and simple dem depression-filling algorithm based on priority queue structure," *Atmospheric and Oceanic Science Letters*, vol. 2, no. 4, pp. 214–219, 2009.
- [33] X. Miao, X. Qiu, S.-S. Wu, J. Luo, D. Gouzie, and H. Xie, "Developing efficient procedures for automated sinkhole extraction from lidar dems," *Photogrammetric Engineering and Remote Sensing*, vol. 79, pp. 545–554, 06 2013.
- [34] J. Zhu, T. P. Taylor, J. C. Currens, and M. M. Crawford, "Improved karst sinkhole mapping in kentucky using lidar techniques: A pilot study in floyds fork watershed," *Journal of Cave & Karst Studies*, vol. 76, no. 3, 2014.

- [35] Y. J. Kim, B. H. Nam, and H. Youn, "Sinkhole detection and characterization using lidar-derived dem with logistic regression," *Remote Sensing*, vol. 11, no. 13, p. 1592, 2019.
- [36] A. Bernatek-Jakiel and M. Jakiel, "Identification of soil piping-related depressions using an airborne lidar dem: Role of land use changes," *Geomorphology*, vol. 378, p. 107591, 2021.
- [37] H. Chen, T. Oguchi, and P. Wu, "A semi-automatic model for sinkhole identification in a karst area of zhijin county, china," in *International Conference on Intelligent Earth Observing and Applications 2015*, vol. 9808, pp. 209–216, SPIE, 2015.
- [38] J. B. Lindsay and I. F. Creed, "Distinguishing actual and artefact depressions in digital elevation data," *Computers & Geosciences*, vol. 32, no. 8, pp. 1192–1204, 2006. Spatial Modeling for Environmental and Hazard Management.
- [39] A. Yavariabdi, H. Kusetogullari, O. Orhan, E. Uray, V. Demir, T. Celik, and E. Mendi, "Sinkholenet: A novel rgb-slope sinkhole dataset and deep weakly-supervised learning framework for sinkhole classification and localization," *The Egyptian Journal of Remote Sensing and Space Sciences*, vol. 26, no. 4, pp. 966–973, 2023.
- [40] N. Kariminejad, A. Mondini, M. Hosseinalizadeh, F. Golkar, and H. R. Pourghasemi, "Detection of sinkholes and landslides in a semi-arid environment using deep-learning methods, uav images, and topographical derivatives," 2023.
- [41] M. U. Rafique, J. Zhu, and N. Jacobs, "Automatic segmentation of sinkholes using a convolutional neural network," *Earth and Space Science*, vol. 9, no. 2, p. e2021EA002195, 2022.
- [42] A. Mihevc and R. Mihevc, "Morphological characteristics and distribution of dolines in slovenia, a study of a lidar-based doline map of slovenia," *Acta Carsologica*, vol. 50, May 2021.
- [43] G. Zhu, Y. Niu, L. Ruan, and X. Zhang, "Amfenet: An adaptive multiscale feature fusion enhancement network for sinkhole detection," *IEEE Geoscience and Remote Sensing Letters*, vol. 21, pp. 1–5, 2024.
- [44] Y. Kim, H. Jung, D. Min, and K. Sohn, "Deep monocular depth estimation via integration of global and local predictions," *IEEE Transactions on Image Processing*, vol. 27, no. 8, pp. 4131–4144, 2018.
- [45] C. Godard, O. Mac Aodha, and G. J. Brostow, "Unsupervised monocular depth estimation with left-right consistency," in *Proceedings of the IEEE conference on computer vision and pattern recognition*, pp. 270–279, 2017.
- [46] P. Pinggera, D. Pfeiffer, U. Franke, and R. Mester, "Know your limits: Accuracy of long range stereoscopic object measurements in practice," in *Computer Vision – ECCV 2014* (D. Fleet, T. Pajdla, B. Schiele, and T. Tuytelaars, eds.), (Cham), pp. 96–111, Springer International Publishing, 2014.
- [47] F. Liu, C. Shen, and G. Lin, "Deep convolutional neural fields for depth estimation from a single image," *CoRR*, vol. abs/1411.6387, 2014.
- [48] V.-C. Miclea and S. Nedevschi, "Monocular depth estimation with improved long-range accuracy for uav environment perception," *IEEE Transactions on Geoscience and Remote Sensing*, vol. 60, pp. 1–15, 2022.
- [49] L. Madhuanand, F. Nex, and M. Y. Yang, "Deep learning for monocular depth estimation from uav images," *ISPRS Annals of the Photogrammetry, Remote Sensing and Spatial Information Sciences*, vol. V-2-2020, pp. 451–458, 2020.
- [50] R. Birkel, D. Wofk, and M. Müller, "Midas v3.1 – a model zoo for robust monocular relative depth estimation," 2023.
- [51] L. Yang, B. Kang, Z. Huang, X. Xu, J. Feng, and H. Zhao, "Depth anything: Unleashing the power of large-scale unlabeled data," 2024.
- [52] J. Zhang, J. Li, Y. Huang, Y. Wang, J. Zheng, L. Shen, and Z. Cao, "Towards robust monocular depth estimation in non-lambertian surfaces," *arXiv preprint arXiv:2408.06083*, 2024.
- [53] D. R. Cambrin, I. Corley, and P. Garza, "Depth any canopy: Leveraging depth foundation models for canopy height estimation," *arXiv preprint arXiv:2408.04523*, 2024.
- [54] L. Zhang, X. Deng, and Y. Lu, "Segment anything model (sam) for medical image segmentation: A preliminary review," in *2023 IEEE International Conference on Bioinformatics and Biomedicine (BIBM)*, pp. 4187–4194, 2023.
- [55] X. Zhang, C. Gu, and S. Zhu, "Sam-helps-shadow: when segment anything model meet shadow removal," 2023.
- [56] A. Archit, S. Nair, N. Khalid, P. Hilt, V. Rajashekar, M. Freitag, S. Gupta, A. Dengel, S. Ahmed, and C. Pape, "Segment anything for microscopy," *bioRxiv*, 2023.
- [57] M. Ahmadi, A. G. Lonbar, A. Sharifi, A. T. Beris, M. Nouri, and A. S. Javidi, "Application of segment anything model for civil infrastructure defect assessment," *arXiv preprint arXiv:2304.12600*, 2023.
- [58] I. Giannakis, A. Bhardwaj, L. Sam, and G. Leontidis, "A flexible deep learning crater detection scheme using segment anything model (sam)," *Icarus*, vol. 408, p. 115797, 2024.
- [59] S. Shankar, L. A. Stearns, and C. van der Veen, "Semantic segmentation of glaciological features across multiple remote sensing platforms with the segment anything model (sam)," *Journal of Glaciology*, pp. 1–10, 2023.
- [60] W. Feng, F. Guan, C. Sun, and W. Xu, "Road-sam: Adapting the segment anything model to road extraction from large very-high-resolution optical remote sensing images," *IEEE Geoscience and Remote Sensing Letters*, vol. 21, pp. 1–5, 2024.
- [61] X. Ma, Q. Wu, X. Zhao, X. Zhang, M.-O. Pun, and B. Huang, "Sam-assisted remote sensing imagery semantic segmentation with object and boundary constraints," *IEEE Transactions on Geoscience and Remote Sensing*, vol. 62, pp. 1–16, 2024.
- [62] O. Rafaeli, T. Svoray, R. Blushtein-Livnon, and A. Nahlieli, "Prompt-based segmentation at multiple resolutions and lighting conditions using segment anything model 2," 2024.
- [63] N. Ravi, V. Gabeur, Y.-T. Hu, R. Hu, C. Ryali, T. Ma, H. Khedr, R. Rädle, C. Rolland, L. Gustafson, et al., "Sam 2: Segment anything in images and videos," *arXiv preprint arXiv:2408.00714*, 2024.
- [64] R. I. Sultan, C. Li, H. Zhu, P. Khanduri, M. Brocanelli, and D. Zhu, "Geosam: Fine-tuning sam with sparse and dense visual prompting for automated segmentation of mobility infrastructure," 2024.
- [65] C. Hetang, H. Xue, C. Le, T. Yue, W. Wang, and Y. He, "Segment anything model for road network graph extraction," 2024.
- [66] R. Sahay and A. Savakis, "On aligning SAM to remote sensing data," in *Geospatial Informatics XIV* (K. Palaniappan and G. Seetharaman, eds.), vol. 13037, p. 1303703, International Society for Optics and Photonics, SPIE, 2024.
- [67] S. Pandey, K.-F. Chen, and E. B. Dam, "Comprehensive multimodal segmentation in medical imaging: Combining yolov8 with sam and hq-sam models," in *Proceedings of the IEEE/CVF international conference on computer vision*, pp. 2592–2598, 2023.
- [68] A. Khatua, A. Bhattacharya, A. K. Goswami, and B. H. Aithal, "Developing approaches in building classification and extraction with synergy of yolov8 and sam models," *Spatial Information Research*, pp. 1–20, 2024.
- [69] F. Trujillano, G. Jimenez, E. Manrique, N. F. Kahamba, F. Okumu, N. Apollinaire, G. Carrasco-Escobar, B. Barrett, and K. Fornace, "Using image segmentation models to analyse high-resolution earth observation data: new tools to monitor disease risks in changing environments," *International Journal of Health Geographics*, vol. 23, no. 1, p. 13, 2024.
- [70] R. Glatt and S. Liu, "Topological data analysis guided segment anything model prompt optimization for zero-shot segmentation in biological imaging," 2023.
- [71] Israel Meteorological Service, "Meteorological data and reports." <https://ims.gov.il>, n.d. n.d.
- [72] I. Stavi and E. Argaman, "Soil quality and aggregation in runoff water harvesting forestry systems in the semi-arid israeli negev," *CATENA*, vol. 146, pp. 88–93, 2016. Dan H. Yaalon Memorial Issue.
- [73] A. Nahlieli, T. Svoray, and E. Argaman, "Piping formation and distribution in the semi-arid northern negev environment: A new conceptual model," *CATENA*, vol. 213, p. 106201, 2022.
- [74] C. E. S. R. I. Redlands, "Arcgis desktop: Release 10," 2011.
- [75] C.-Y. Yang, I.-H. Yeh, and H.-Y. M. Liao, "Yolov9: Learning what you want to learn using programmable gradient information," 2024.
- [76] J. Ma, Y. He, F. Li, L. Han, C. You, and B. Wang, "Segment anything in medical images," *Nature Communications*, vol. 15, Jan. 2024.
- [77] A. Bonnet, "Learn how to fine-tune the segment anything model (sam)," *Encord Blog*, April 2023. Accessed: 2024-09-04.
- [78] G. Jocher, A. Chaurasia, and J. Qiu, "Ultralytics yolo," jan 2023. Available: <https://github.com/ultralytics/ultralytics>.
- [79] J. Wall, D. Bohnenstiehl, K. Wegmann, and N. Levine, "Morphometric comparisons between automated and manual karst depression inventories in apalachicola national forest, florida, and mammoth cave national park, kentucky, usa," *Natural Hazards*, vol. 85, 01 2017.
- [80] R. Blushtein-Livnon, T. Svoray, and M. Dorman, "Performance of human annotators in object detection and segmentation of remotely sensed data," 2024.
- [81] H. Chen, T. Oguchi, and P. Wu, "Morphometric analysis of sinkholes using a semi-automatic approach in zhijin county, china," *Arabian Journal of Geosciences*, vol. 11, 08 2018.
- [82] B. Du, Z. Wang, L. Zhang, L. Zhang, W. Liu, J. Shen, and D. Tao, "Exploring representativeness and informativeness for active learning," *IEEE Transactions on Cybernetics*, vol. 47, no. 1, pp. 14–26, 2017.

- [83] O. Rafaeli, A. Nahlieli, and T. Svoray, "Dynamics of subsurface soil erosion in a semiarid region: A time-series study of sinkhole area and morphology," *CATENA*, vol. 233, p. 107511, 2023.
- [84] Z. Jiang, S. Hu, H. Deng, N. Wang, F. Zhang, L. Wang, S. Wu, X. Wang, Z. Cao, Y. Chen, *et al.*, "Detection and automatic identification of loess sinkholes from the perspective of lidar point clouds and deep learning algorithm," *Geomorphology*, p. 109404, 2024.
- [85] W. Ji, J. Li, Q. Bi, T. Liu, W. Li, and L. Cheng, "Segment anything is not always perfect: An investigation of sam on different real-world applications," 2024.



Osher Rafaeli received a B.Sc. in Geology from Ben-Gurion University of the Negev (BGU), Beer Sheva, Israel, in 2018. He is currently a Ph.D. student at the Ben-Gurion University of the Negev. His main research interests include AI-based image processing and geoinformatics solutions for soil piping erosion research.



Tal Svoray received a Ph.D. in Radar Remote Sensing of Mediterranean Vegetation from Bar Ilan University, Ramat-Gan, Israel, in 2001. He is currently a Professor at the Ben-Gurion University of the Negev. His main research interests include object segmentation and detection, remote sensing of soil and vegetation, environmental psychology and geostatistics..

Ariel Nahlieli received a Ph.D. from the Department of Environmental, Geoinformatics and Urban Planning Sciences at Ben-Gurion University of the Negev, Beer Sheva, Israel, in 2024. He is currently focused on researching and understanding the main factors that contribute to the formation and evolution of soil piping erosion in semiarid regions.